Cell-specific Cahn-Hilliard models predict condensed fates of the chromosomal passenger complex

Sarah Groves[1] · Catalina Alvarez[1] · Min-Jhe Liu[2] · Montserrat Gerardo[1] · John Lowengrub[2] · Todd Stukenberg[1] · Kevin Janes[1]

[1]Department of Biomedical Engineering · UVA [2]Department of Mathematics · UC Irvine

SASCO Center for Systems Analysis of Stress-adapted Cancer Organelles

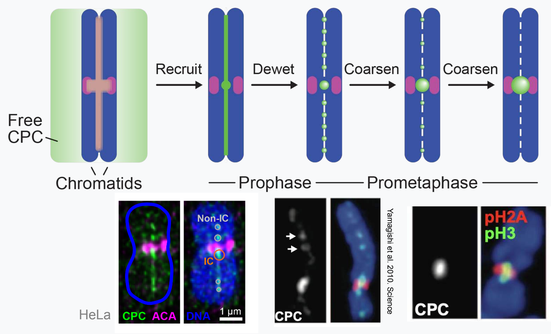
Abstract

Biomolecular condensates create dynamic subcellular compartments that alter systems-level properties of the networks surrounding them and may become dysregulated in cancer. Standard reaction-diffusion models of systems biology cannot define where these compartments emerge nor track how they evolve.

Here, we use an alternative physiochemical model, the **Cahn-Hilliard equation**, to build solvers in three common systems-biology programming languages. We applied these solvers to the chromosomal passenger complex, a multi-protein assembly that reportedly condenses on mitotic chromosomes to ensure proper chromosomal segregation.

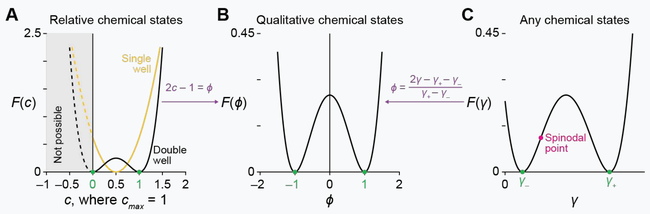
The simulation results suggest how initially variegated recruitment yields robust localization of the chromosomal passenger complex (CPC) to the inner centromere. Cancer can lead to perturbed abundances of proteins in a signaling network centered on CPC. Integration with a reaction-diffusion model using VCell delineates the dysregulation of the CPC signaling network and condensation, and thus chromosomal segregation, in breast cancer.

Introduction / Background



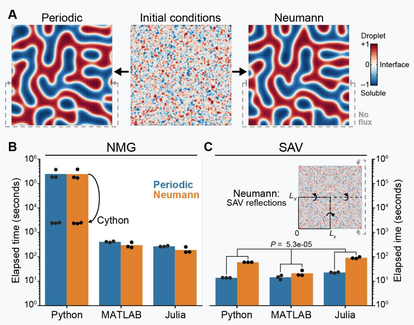
Top: CPC recruitment to the IC during prophase and prometaphase. Freely diffusible CPC (green) and chromatin bound CPC is recruited strongly to the IC between kinetochores (magenta) and less so between sister chromatids. During late prophase, CPC dewets into discrete foci, which coarsen until all CPC is IC-localized by prometaphase.
Bottom: Immunofluorescence illustrations of CPC dewetting on chromosomes stained for AURKB (a CPC subunit), anti-centromeric antigen (ACA), and DAPI to label DNA (blue).

$$\frac{\partial \phi}{\partial t} = D\nabla^2\mu = D\nabla^2\left(\frac{dF}{d\phi} - \epsilon_m^2\nabla^2\phi\right)$$



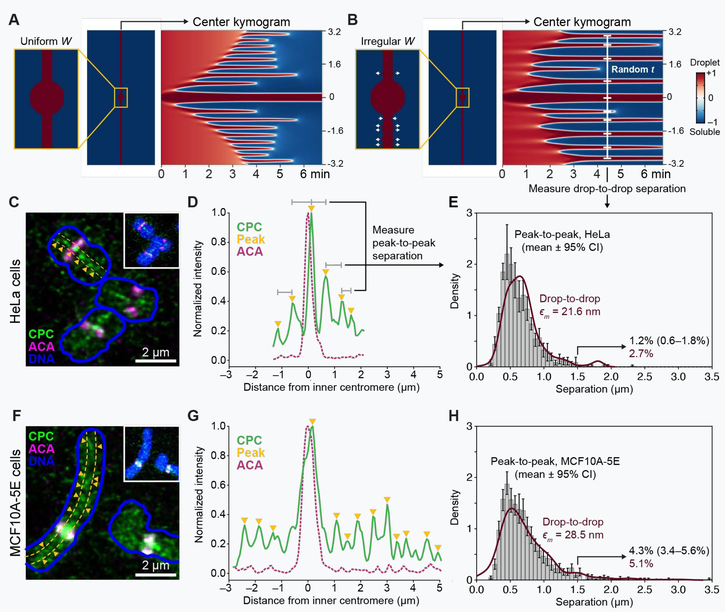
The Cahn-Hilliard double-well free energy function (F) accommodates differences in location and scale. (A) Comparison of a single-well function (yellow, with cavg = 0.5) and a double-well function (black, stable states at 0 and 1 in green). (B) The double-well function of (A) is made symmetric about the y-axis with linear shifts and scaling (purple). (C) Any pair of chemical states (γ– and γ+ in green) is similarly shifted and scaled to (B). The spinodal point (magenta) is constrained.

Cahn Hilliard Solver Performance



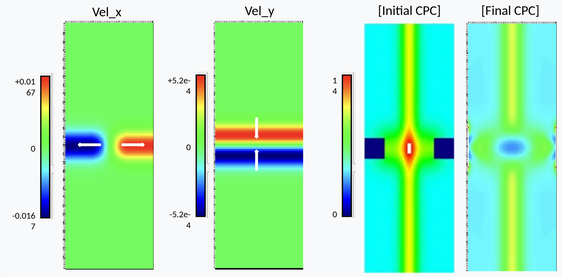
Computing performance depends on the programming language for NMG and the boundary condition for SAV. (A) Snapshots of spinodal decomposition when boundary conditions are periodic (left), whereby flux exiting one edge enters on the opposite edge, or Neumann (right) specifying zero flux at the edges. (B, C) Runtime performance for NMG (B) and SAV (C) solvers in Python, MATLAB, and Julia for spinodal decompositions initialized with N = 3 random mixtures of ±1 chemical states (25:75, 50:50, and 75:25) and either periodic or Neumann boundary conditions. For NMG, the Cython implementation is shown relative to. For SAV, Neumann boundary conditions require X and Y reflections to re-establish periodic boundaries for the expanded spatial domain (C, inset). Boundary conditions in (C) were tested by multiway ANOVA with boundary condition and programming language as factors. All simulations were performed on AMD EPYC 9454 processors (3.81 GHz max, 48 cores per socket, 2 sockets) with up to 500 GB RAM allocated, using up to 16 cores for computation on a 27 Å~ 27 mesh for 2000 time steps (dt = 5.5e-6) with cm = 8.

Chromatin-bound CPC behaves as a phase-separated Cahn-Hilliard fluid

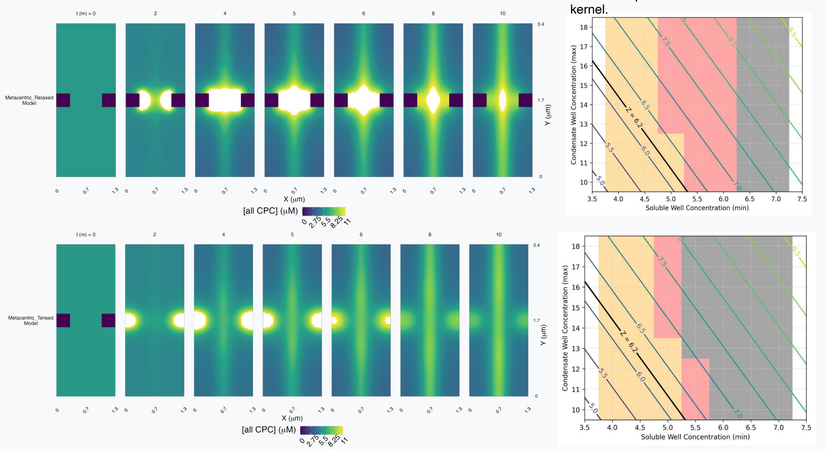


(A, B) Kymogram illustration of central droplets for 6.8 minutes after initialization with RIC = 150 nm and W = 90 nm (A) or 90 ± 10 nm (B, white arrows). Drop-to-drop distances were quantified at randomly selected times t. (C) Immunofluorescence staining of dewetted CPC on HeLa chromosomes after G2 release for 10 minutes. (D) Normalized intensity of AURKB and ACA for the HeLa chromosome in (C). (E) Comparison of bootstrapped peak-to-peak separation of CPC foci in HeLa cells (gray histogram) with drop-to-drop distances from Cahn-Hilliard simulations with cm = 21.6 nm (red line). (F) Immunofluorescence staining of dewetted CPC on MCF10A-5E chromosomes after G2 release for 70 minutes. (G) Normalized intensity of AURKB and ACA for the MCF10A-5E chromosome in (F). (H) Comparison of bootstrapped peak-to-peak separation of CPC foci in MCF10A-5E cells (gray histogram) with drop-to-drop distances from Cahn- Hilliard simulations with cm = 28.5nm (red line). For (C, F), cells were stained for AURKB (a CPC subunit; green), anti-centromeric antigen (ACA; magenta), and DAPI to label DNA (blue). A 300-nm thick axial line scan (dotted yellow line) was used to identify peaks of AURKB foci (yellow triangles; Materials and Methods). For (D, G), normalized fluorescence intensities are shown relative to distance from the inner centromere based on the peak ACA location centered at zero. Peaks of AURKB foci (yellow triangles) were identified with a computational algorithm (Materials and Methods) and quantified. For (E, H), data are shown as the median ± 95% bootstrapped confidence interval (CI) from N = 221 chromosomes in 10 cells (E) or 216 chromosomes in 50 cells (H). The fraction of predicted (red) and measured (black) separations greater than 1.5 μm is indicated.

Cahn Hilliard condensation phase field: qualitative outcomes of CPC network dynamics



CPC bound to chromatin mesh senses tension emanating from deformable kinetochores. The relaxed-to-tensed transition was modeled by advecting kinetochores 300 nm horizontally in opposite directions at a constant peak velocity of 0.0167 μm/sec. The peak velocity declined to zero at the inner centromere by applying a horizontal Gaussian kernel with σ_x matching the distance traveled by the kinetochores and a normalization factor ensuring peak velocity at the kinetochore. To capture kinetochore deformability, the peak velocity at the kinetochore center was smoothed using a vertical Gaussian kernel with σ_y equal to one half of the kinetochore height (150 nm in the base model). The mitotic chromatin of the inner centromere was modeled as a self-entangled gel with partial compressibility. Stretching in X led to compression in Y with a Poisson ratio of 0.3, which was applied vertically as a V-shaped kernel multiplied with the earlier Gaussian kernel.



Top: Relaxed state model simulation with no tension at kinetochores shows CPC accumulation in the inner centromere. A parameter scan over the soluble and condensate well concentrations (see introduction) shows regions of stable, decreasing, and dissolved droplets after Cahn Hilliard modeling from [CPC] at 5 minutes. Bottom: Same for the transition-to-tensed model, where the stretching due to proper KT-MT attachments occurs at t=0s. After 5 minutes, the Cahn Hilliard modeling shows a propensity to dissolved droplets.

Conclusions & Future Directions

- Advection of deformable kinetochores attached to a compressible elastic mesh of chromatin models biological stretching under tension
- Cahn Hilliard simulations provide qualitative outcomes of chromosomes stretched by proper attachments to the spindle
- Advection + Cahn Hilliard simulations explain tensometer behavior of CPC condensates

Funding from SASCO Center: NCI U54 CA274499